THREE-DIMENSIONAL NONLINEAR HYDRODYNAMICS CODE TO STUDY LASER–PLASMA INTERACTIONS

C. H. Still *R. L. Berger*

A. B. Langdon *E. A. Williams*

Introduction

The development of a fully nonlinear, time-dependent hydrodynamic and heat transport code has allowed us to pursue several very interesting problems in laser beam self-focusing and filamentation for which the plasma density and flow velocities are strongly perturbed. Many treatments have used time-dependent linearized hydrodynamics in two and three dimensions (3-D) where the plasma motion is limited to directions transverse to the laser propagation direction.[1,2] A truly nonlinear treatment uses particle-in-cell codes.[3] Other nonlinear treatments have used a steady-state hydrodynamics response where the electron density is determined by equating the electron thermal and ponderomotive forces transverse to the laser propagation direction.[4]

These approaches ignore some important physical processes. For example, time-dependent, nonlinear hydrodynamics is needed to address steepening of wave fronts, harmonic generation and decay instabilities, all of which play an important role in saturation of filamentation, stimulated Brillouin scattering (SBS), and stimulated Raman scattering (SRS). Filamentation has been studied using 1-D and 2-D nonlinear hydrodynamics codes in planar or cylindrical geometry.[5] To our knowledge, the code we now describe is the only code with fully 3-D nonlinear hydrodynamics coupled to light wave propagation.

The Hydrodynamics Equations

The hydrodynamic, heat transport equations in conservative form are the mass conservation equation

$$\frac{\partial}{\partial t}\rho + \nabla\cdot(\mathbf{v}\rho) = 0 \quad , \tag{1}$$

the momentum conservation equation for the j^{th} component of the momentum $\mathbf{S}$

$$\frac{\partial}{\partial t}S_j + \nabla\cdot(\mathbf{v}S_j) + \nabla\cdot\mathbf{Q}_j + \frac{\partial}{\partial x_j}P + \frac{\partial}{\partial x_j}P_e + \rho\frac{\partial}{\partial x_j}\varphi = 0 \quad , \tag{2}$$

the ion energy conservation equation

$$\frac{3}{2}\left[\frac{\partial}{\partial t}P + \nabla\cdot(\mathbf{v}P)\right] + P\,\nabla\cdot\mathbf{v} + \mathbf{Q}:\nabla\mathbf{v} = 0 \quad , \tag{3}$$

and the electron energy conservation equation

$$\frac{3}{2}\left[\frac{\partial}{\partial t}P_e + \nabla\cdot(\mathbf{v}P_e)\right] + P_e\,\nabla\cdot\mathbf{v} = -\nabla\cdot\mathbf{q}_e + H_e \quad . \tag{4}$$

In these equations, P is the ion pressure, P_e is the electron pressure, $\mathbf{Q}$ is the viscosity tensor (with j^{th} component $\mathbf{Q}_j$), $\mathbf{v}$ is the flow velocity, H_e is a source or sink, and $\mathbf{q}_e$ is the heat flow. The momentum is related to the flow velocity by

$$\mathbf{S} = \rho\mathbf{v} \quad , \tag{5}$$

and the electron and ion temperature are related to the corresponding pressures by a perfect gas equation of state

$$P_e = n_e T_e \tag{6}$$

$$P = n_i T_i \tag{7}$$

with $\rho = m_i n_i$. The ionization state is constant and, at present, quasi-neutrality is assumed, namely $n_e = Z n_i$. This last assumption will be relaxed in the near future.

The last term in the momentum equation [Eq. (2)] represents either a gravitation force, as used for

Rayleigh–Taylor instability calculations,[6] or a ponderomotive force, in which case

$$\varphi = \frac{1}{2}\frac{m_i}{Zm_e}|\mathbf{v}_0|^2 \quad . \tag{8}$$

Here, $\mathbf{v}_0$ is the jitter velocity of the electron in the laser field $\mathbf{E}_0$,

$$\mathbf{v}_0 = \frac{e\mathbf{E}_0}{m_e\omega_0} \quad . \tag{9}$$

In Eq. (3), we neglect the ion heat flow and real viscosity, which are usually very small. The artificial viscosity **Q** is used to handle shocks in the standard way as will be described shortly.

In Eq. (4), H_e includes collisional heating (inverse bremsstrahlung). For problems of interest to date, the standard flux-limited heat flow

$$\mathbf{q}_e = -\kappa(T_e)\ \nabla T_e \tag{10}$$

where

$$\kappa(T_e) = \min\left(\kappa_{SH}, fn_e v_e T_e \frac{|\nabla T_e|}{T_e}\right) \tag{11}$$

is ineffective in limiting the heat flow because the gradients in T_e are small over the scales of interest to filamentation. On the other hand, nonlocal transport[7] can be quite important. Unfortunately, a nonlinear, nonlocal 3-D treatment of electron transport is a research project in itself. Thus, we have taken the approach of linearizing Eq. (4) about a uniform T_{e0} to obtain $\delta T_e = T_e - T_{e0}$, which is calculated from nonlocal electron transport. The choice for T_{e0} has come either from experimental data or from LASNEX simulations. In most cases of interest, this approximation has been satisfactory. It becomes questionable when there are large excursions in density because of the concomitant large excursions in electron–ion and electron–electron scattering mean-free-paths. Fortunately, in most applications with such large excursions, self-focusing is ponderomotively driven rather than thermally driven. Electron–ion energy exchange terms have been dropped in Eqs. (3) and (4) because they are of interest only for nanosecond time scales; in general, filamentation time scales are much shorter.

For completeness, we include the equation for the light wave propagation given by the modified paraxial equation

$$\left(\frac{\partial}{\partial t} + v_g\frac{\partial}{\partial z} - \frac{ic^2}{2\omega_0}D^2 + \nu\right)E = -\frac{4\pi e^2 i}{2\omega_0 m_e}\delta n_e E \tag{12}$$

for the complex light-wave envelope amplitude E oscillating at frequency ω_0 and wave vector

$$c^2 k_z^2 = \frac{4\pi e^2}{m_e}\bar{n}_e - \omega_0^2 \quad . \tag{13}$$

Here, we define

$$\bar{n}_e(z) = \langle n_e(x,y,z)\rangle_{xy} \quad , \tag{14}$$

$$\delta n_e = n_e(x,y,z) - \bar{n}_e(z) \quad , \tag{15}$$

the light wave group velocity

$$v_g(z) = \frac{c^2 k_0(z)}{\omega_0} \quad , \tag{16}$$

the inverse bremsstrahlung absorption rate ν and the generalized diffraction operator[8]

$$D^2 = \frac{2k_0 - \nabla^2}{k_0 + \sqrt{k_0^2 - \nabla^2}} \quad , \tag{17}$$

which extends validity of the paraxial equation to higher order in ∇. The numerical solution of Eq. (12) is described by Berger et al.[2]

Numerical Solution of the Hydrodynamical Equations

We followed the procedure outlined by Bowers and Wilson[9] and implemented by Miller in 2-D for spherical or cylindrical geometry.[10] Our code, called NH3 if uncoupled to laser light, or F3D when coupled to laser light, is 3-D Cartesian to match the fast Fourier transform (FFT) solution techniques used for the light equation solver.

The advection steps in the continuity and energy equations [Eqs. (1) and (3)] are done similarly. The equation is split into three 1-D equations, which are solved successively,

$$\frac{\partial}{\partial t}\rho^{(+1/3)} = -\frac{\partial}{\partial x}\left(\rho^{(+0)}v_x\right) \tag{18}$$

$$\frac{\partial}{\partial t}\rho^{(+2/3)} = -\frac{\partial}{\partial y}\left(\rho^{(+1/3)}v_y\right) \tag{19}$$

$$\frac{\partial}{\partial t}\rho^{(+1)} = -\frac{\partial}{\partial z}\left(\rho^{(+2/3)}v_z\right) \tag{20}$$

where $\rho^{(+0)}$ and $\rho^{(+1)}$ denote the actual time-iterates, and the other two quantities are intermediate results. The advection is done by a 1-D scheme,

$$\rho_{i-1/2}^{(t+1)} = \rho_{i-1/2}^{(t)} + \left(F_i^{M_x} - F_{i+1}^{M_x}\right)/\Delta x \tag{21}$$

$$F_i^{M_x} = \hat{\rho}_i \bar{v}_i \Delta t \tag{22}$$

$$\bar{v}_i = \frac{1}{4}\left(v_{i,j,k} + v_{i,j+1,k} + v_{i,j,k+1} + v_{i,j+1,k+1}\right) \quad , \tag{23}$$

where the subscripts denote spatial position, using Van Leer's second-order upwind monotonic approximation for $\hat{\rho}$.[9,11] The Van Leer method defines

$$\rho_{\max} = \max\left(\rho_{i-3/2}, \rho_{i-1/2}, \rho_{i+1/2}\right) \tag{24}$$

$$\rho_{\min} = \min\left(\rho_{i-3/2}, \rho_{i-1/2}, \rho_{i+1/2}\right) \tag{25}$$

$$\Delta\rho_1 = 2\,\min\left(\rho_{\max} - \rho_{i-1/2}, \rho_{i-1/2} - \rho_{\min}\right) \tag{26}$$

$$\Delta\rho_2 = \frac{1}{2}\left(\rho_{i+1/2} - \rho_{i-3/2}\right) \tag{27}$$

$$\Delta\rho_3 = \max\left(\rho_{\max} - \rho_{i-1/2}, -\rho_{i-1/2} - \rho_{\min}, |\Delta\rho_2|\right) \tag{28}$$

$$\delta_{i+1/2} = \mathrm{sign}\left(\Delta\rho_2\right)\min\left(\Delta\rho_1, \Delta\rho_3\right) / \Delta x \tag{29}$$

$$\hat{\rho}_i = \begin{cases} \rho_{i-1/2} + \frac{1}{2}\delta_{i-1/2}\left(\Delta x - v_i \Delta t\right), & \text{if } v_i > 0 \\ \rho_{i+1/2} - \frac{1}{2}\delta_{i+1/2}\left(\Delta x + v_i \Delta t\right), & \text{otherwise} \end{cases} \quad . \tag{30}$$

This scheme guarantees a non-negative density.

Pressure changes due to mechanical work on a cell and artificial viscosity are handled separately. As with mass continuity, the energy equation is split into three 1-D equations to be solved successively, similar to Eqs. (17)–(20):

$$\frac{\partial}{\partial t} P^{(+1/3)} = -\frac{\partial}{\partial x}\left(\hat{P}^{(+0)} v_x\right) \quad , \mathrm{etc} \tag{31}$$

Transport is done by a 1-D scheme similar to the mass equation:

$$P_i^{(t+1)} = P_i^{(t)} + \left(F_i^P - F_{i+1}^P\right) / \Delta x \tag{32}$$

$$F_i^P = \hat{P}_i \bar{v}_i \Delta t \tag{33}$$

$$\bar{v}_i = \frac{1}{4}\left(v_{i,j,k} + v_{i,j+1,k} + v_{i,j,k+1} + v_{i,j+1,k+1}\right) \tag{34}$$

where $\hat{P}$ is computed exactly the same way as $\hat{\rho}$. The $P\ \cdot\mathbf{v}$ (PdV work) and artificial viscosity at $t + \Delta t$ are done given the momentum equation solution, which is at time level $t + \frac{\Delta t}{2}$.

Again, each component of momentum is advected separately, e.g.,

$$\frac{\partial}{\partial t} S_x + \frac{\partial}{\partial x}\left(v_x S_x\right) + \frac{\partial}{\partial y}\left(v_y S_x\right) + \frac{\partial}{\partial z}\left(v_z S_x\right) = 0 \quad . \tag{35}$$

Artificial viscosity, pressure gradients, and ponderomotive force are each treated separately, and transport is done by an advection scheme:

$$\begin{aligned} \left(S_x^{t+1}\right)_{i,j,k} = {} & \left[S_x^{(t)}\right]_{i,j,k} \\ & + \left[\left(F_x^{S_x}\right)_{i-1/2,j,k} - \left(F_x^{S_x}\right)_{i+1/2,j,k}\right] / \Delta x \\ & + \left[\left(F_x^{S_y}\right)_{i,j-1/2,k} - \left(F_x^{S_y}\right)_{i,j+1/2,k}\right] / \Delta y \\ & + \left[\left(F_x^{S_z}\right)_{i,j,k-1/2} - \left(F_x^{S_z}\right)_{i,j,k+1/2}\right] / \Delta z \quad , \end{aligned} \tag{36}$$

where

$$\left(F_x^{S_x}\right)_{i-1/2,j,k} = \left(\hat{v}_x\right)_{i-1/2,j,k} \bar{F}^{M_x}_{i+1/2,j-1/2,k-1/2} \tag{37}$$

$$\left(F_x^{S_y}\right)_{i-1/2,j,k} = \left(\hat{v}_y\right)_{i-1/2,j,k} \bar{F}^{M_x}_{i+1/2,j-1/2,k-1/2} \tag{38}$$

$$\left(F_x^{S_z}\right)_{i-1/2,j,k} = \left(\hat{v}_z\right)_{i-1/2,j,k} \bar{F}^{M_x}_{i+1/2,j-1/2,k-1/2} \quad . \tag{39}$$

$\bar{F}^{M_x}$ denotes the average mass-flux in the x-direction over the cell, and $\hat{v}_x, \hat{v}_y$, and $\hat{v}_z$ are computed using a slight modification of the Van Leer method defined in Eqs. (24)–(30) [the slope $\Delta\rho_3$ is excluded from Eq. (29)]:

$$\delta_i = \mathrm{sign}\left(\Delta v_2\right)\min\left(\Delta v_1, |\Delta v_2|\right) / \Delta x \quad . \tag{40}$$

After the transport step is complete, the change in momentum from thermal pressure gradients

$$\frac{\partial}{\partial t} S_x = -\frac{\partial}{\partial x} P \tag{41}$$

$$\left(S_x\right)_{i,j,k}^{(t+1)} = \left(S_x\right)_{i,j,k}^{(t)} - \frac{\Delta t}{\Delta x}\left(\bar{P}_{i+1/2,j,k} - \bar{P}_{i-1/2,j,k}\right) \tag{42}$$

$$\begin{aligned} \bar{P}_{i+1/2,j,k} = {} & \left(P_{i+1/2,j-1/2,k-1/2} + P_{i+1/2,j+1/2,k-1/2}\right. \\ & + P_{i+1/2,j-1/2,k+1/2} \\ & \left. + P_{i+1/2,j+1/2,k+1/2}\right) / 4 \end{aligned} \tag{43}$$

and ponderomotive forces

$$\frac{\partial}{\partial t} S_x = -\rho \frac{\partial}{\partial x} \varphi \tag{44}$$

$$\left(S_x\right)_{i,j,k}^{(t+1)} = \left(S_x\right)_{i,j,k}^{(t)} - \frac{\Delta t}{\Delta x} \bar{\rho}_{i,j,k} \left(\bar{\varphi}_{i+1/2,j,k} - \bar{\varphi}_{i-1/2,j,k}\right) \tag{45}$$

$$\begin{aligned} \bar{\varphi}_{i+1/2,j,k} = (&\varphi_{i+1/2,\,j-1/2,\,k-1/2} + \varphi_{i+1/2,j+1/2,k-1/2} \\ &+ \varphi_{i+1/2,j-1/2,k+1/2} \\ &+ \varphi_{i+1/2,j+1/2,k+1/2}) / 4 \end{aligned} \tag{46}$$

is calculated, where $\bar{\rho}$ is the average over the cell.

The artificial viscosity is handled similarly and has the form

$$\left(Q_{xx}\right)_{i+1/2} = \begin{cases} C_Q \rho_{i+1/2} \left[\left(\Delta v_x\right)_{i+1/2}\right]^2, & \text{if} \left(\Delta v_x\right)_{i+1/2} < 0 \\ 0, & \text{otherwise} \end{cases} \tag{47}$$

where

$$\left(\Delta v_x\right)_{i+1/2} = \left(\bar{v}_x\right)_{i+1} - \left(\bar{v}_x\right)_i \tag{48}$$

and $\bar{v}_x$ is the average over the face

$$\left(\bar{v}_x\right)_i = \left[\left(v_x\right)_{i,j,k} + \left(v_x\right)_{i,j+1,k} + \left(v_x\right)_{i,j,k+1} + \left(v_x\right)_{i,j+1,k+1}\right] / 4 \tag{49}$$

Note that we only keep the diagonal elements from the artificial viscosity term in Eq. (2). Through numerical experimentation, we have determined that $C_Q = 1$ is a reasonable choice, even in the presence of fairly steep shocks.

We have also included a time-step controller to allow a larger Δt when possible, but to ensure that the Courant condition is satisfied. In cases where plasma velocities grow an order of magnitude or more from their initial size, the time step is decreased so that the numerical scheme is stable. When coupled to F3D, the time step is never increased beyond the limit specified by the light propagation.

We have tested this hydrodynamics scheme on several different kinds of problems ranging from deflection of a laser beam in a flowing plasma[12] to plasma expansion into a vacuum.[13–14]

Simulation of the Self-Focusing of a High-Intensity Laser Beam

As an example of an interaction in which nonlinear hydrodynamics is important, we show the results of propagating a 1.06-μm laser beam with initial intensity of 10^{16} W/cm^2 through a CH plasma whose initial electron density and temperature are uniform with values of $n_e = 0.1 n_c$ and $T_e = 1$ keV and thus $v_0/v_e = 2$. (These conditions are similar to those reported by Young et al.[15]) The laser electric field amplitude at $z = 0$ is taken to be

$$E(x,y)_{z=0} = \begin{cases} E_0(t) \cos^2\left(\frac{\pi x}{L_x}\right) \cos^2\left(\frac{\pi y}{L_y}\right), & \text{if} |x| \le \frac{L_x}{2}, |y| \le \frac{L_y}{2} \\ 0, & \text{otherwise,} \end{cases} \tag{50}$$

where $L_x = L_y = 40$ μm, $L_z = 100$ μm, $-L_x \le x \le L_x$, $-L_y \le y \le L_y$, and $0 \le z \le L_z$. The amplitude $E_0(t)$ rises from 0 to a constant peak value over 100 ps. The field is periodic in the transverse directions, and outgoing at $z = z_{max}$.

In Fig. 1(a), isocontours of the laser intensity at 252 ps are shown. The contours are 2.5, 4.5, 7.5 × 10^{16} W/cm^2, with the darkest contour being least intense. After propagating about 50 μm, the laser intensity reaches a strong focus with peak intensity $I = 5 \times 10^{17}$ W/cm^2, after which it breaks apart into about four filaments. The initial laser power at $z = 0$ is 100 times the critical power for self-focusing.[16] $P_{crit} = 9 \times 10^8$ W for these conditions, so we might expect the number of filaments $N \approx P/P_{crit} = 100$. The evolution to this highly filamented state requires simulation of a much longer plasma because the distance to focus of a filament varies inversely with power. The distance to the first focus in steady state can be estimated from the steady-state spatial growth rate κ as $L_f = \kappa^{-1} \quad 23\ \lambda_0$ for this case.[17] The steady-state focus actually is achieved at ~50 λ_0.

Isocontours of the electron density associated with this laser intensity distribution are shown in Fig. 1(b).

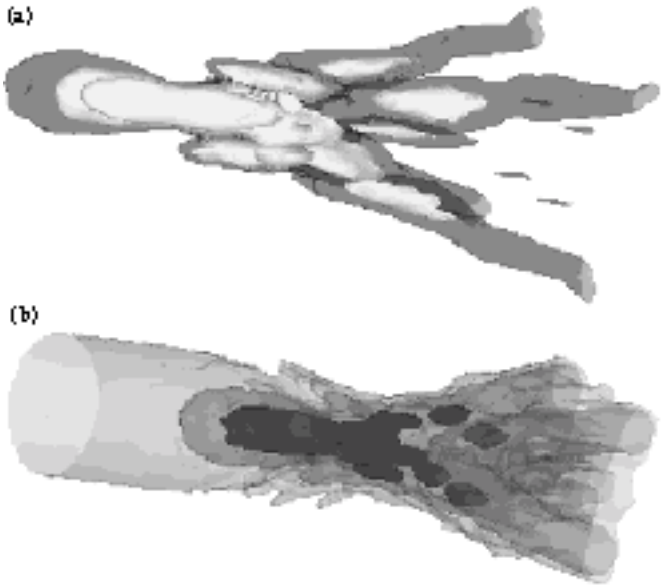

FIGURE 1. (a) Energy intensity contours; (b) density contours. Darkest contours are least intense (a) and least dense (b). (10-00-0896-1932pb01)

The density at the first focus, i.e. peak intensity, is essentially zero: $5 \times 10^{-8}\ n_c$. The contours in Fig. 1(b) are $10^{-2}\ n_c$, $10^{-4} n_c$, and $10^{-5} n_c$, lightest to darkest.

This configuration appears to be near the final state after a very dynamic epoch. The first focus of the laser moves backward at high velocity from $z = 100\ \mu$m at 47 ps to $z = 60\ \mu$m at 55 ps or a velocity of 5×10^8 cm/s. $E_0(t)$ is still increasing during this period. The first focus stays around 55 μm after 60 ps until the end of the simulation at 252 ps.

A number of filamentation codes, including the linearized hydrodynamic version of F3D, neglect the plasma motion along the laser propagation direction because the transverse scale length of the laser hot spot or speckle is much smaller than the axial scale; the ratio of lengths is $8f$ where f is the f-number of the focusing optic. In this simulation the axial flow is important. During the time the focus is moving from $z = 100\ \mu$m to $z = 60\ \mu$m at supersonic velocity, it accelerates the axial flow velocity of the fluid in front of best focus from near 0 to about -3×10^8 cm/s. The ponderomotive force also accelerates plasma supersonically in the positive axial direction at speeds up to 3×10^8 cm/s and transversely at velocities ~6×10^7 cm/s. At the sides of the filaments, the plasma is compressed and heated. The energy in the supersonically moving plasma, when dissipated, results in local ion temperatures in excess of 10 keV. The initial ion temperature was 500 eV.

Summary

As the self-focusing example of Fig. 1 illustrates, filamentation of intense laser beams produces a very nonlinear response in the plasma. The assumptions of a linearized treatment quickly break down. The nonlinear hydrocode described in this article has proven to be very robust and extends our ability to model experiments far beyond the limits of our earlier linear hydrodynamics treatment. Yet further improvements to the physical description are contemplated. The peak intensity achieved at best focus—5×10^{17} W/cm^2 at $\lambda_0 = 1.06\ \mu$m—is weakly relativistic, $v_0^2 / c^2 \approx 0.5$, and suggests that relativistically correct expressions for the ponderomotive force be used.[18] The ions are accelerated to such a high velocity, ~5×10^8 cm/s, that interpenetration[19] rather than stagnation is anticipated at the edges of the evacuated regions associated with filaments. This happens because the ion–ion mean-free-path is estimated in some cases to be larger than the distance over which the flow decelerates. For similar reasons, ion heat conduction should be included in some cases. Inclusion of Poisson's equation might also prove necessary to model the ion–wave dynamics correctly.[20]

Notes and References

1. In addition, the density perturbation is limited in magnitude by replacing the linear response $\delta N = (n - n_0)/n_0$ by $\ln(1 + \delta N)$ so the total density is never negative.
2. R. L. Berger, B. F. Lasinski, T. B. Kaiser, E. A. Williams, et al., *Phys. Fluids B* **5** (7), 2243–2258 (1993); R. L. Berger, B. F. Lasinski, A. B. Langdon, T. B. Kaiser, et al., *Phys. Rev. Lett.* **75** (6), 1078–1081 (1995); S. Hüller et al., "Numerical Simulation of Filamentation and its Interplay with SBS in Underdense Plasmas," submitted to *Physica Scripta* (1996); A. J. Schmitt, *Phys. Fluids* **31** (10), 3079–3101 (1988); A. J. Schmitt, *Phys. FluidsB* **3** (1), 186–194 (1991).
3. A. B. Langdon and B. F. Lasinski, *Phys. Rev. Lett.* **34** (15), 934–937 (1975).
4. M. A. Blain, G. Bonnaud, A. Chiron, and G. Riaguelo, *Autofocalisation de Filamentation d'un Faisceau Laser dans le Cadre de l'Approximation Paraxiale et Stationnaire*, CEA-R-5716; B. I. Cohen et al., *Phys. Fluids B* **3** (3), 766–775 (1991); V. E. Zakharov et al., *Sov. Phys. JEPT* **33** (1), 77–81 (1971).
5. D. Havazelet et al., *Phys. Fluids B* **1** (4), 893–900 (1989); R. Rankin et al., *Phys. Rev. Lett.* **63** (15), 1597–1600 (1989); H. A. Rose, *Phys. Plasmas* **3** (5), 1709–1727 (1996).
6. S. H. Langer, Rayleigh–Taylor calculations.
7. E. M. Epperlein, *Phys. Fluids B* **1** (11), 3082–3086 (1991); T. B. Kaiser, B. I. Cohen, R. L. Berger, B. F. Lasinski et al., *Phys. Plasmas* **1**, 1287 (1994); J. R. Albritton, E. A. Williams, I. B. Bernstein, and K. P. Swartz, *Phys. Rev. Lett.* **57**, 1887 (1986).
8. M. D. Feit and J. A. Fleck, Jr., *J. Opt. Soc. Am. B* **5** (3), 633–640 (1988).
9. R. L. Bowers and J. R. Wilson, *Numerical Modeling in Applied Physics and Astrophysics* (Jones and Bartlett, Boston, MA, 1991), 199–347.
10. D. S. Miller, *Convection in Type II Supernovae*, Ph. D. Thesis (1993).
11. B. Van Leer, *J. Comp. Phys.* **23** (3), 276–299 (1977); B. Van Leer, *J. Comp Phys.* **32** (1), 101–136 (1979).
12. D. Hinkel, E. A. Williams, and C. H. Still, *Phys. Rev. Lett.* **77** (7), 1298–1301 (1996).
13. C. H. Still, R. L. Berger, A. B. Langdon, and D. S. Miller, "Nonlinear Eulerian Hydrodynamics in Three Dimensions," Anomalous Absorption Conference, Aspen, CO (1995).
14. C. H. Still, R. L. Berger, A. B. Langdon, D. S. Miller, and E. A. Williams, "Nonlinear Eulerian Hydrodynamics in 3D," *Bull. APS* **40** (11), (1995).
15. P. E. Young, G. Guethlein, S. C. Wilks, J. H. Hammer, et al., *Phys. Rev. Lett.* **76** (17), 3128–3131 (1996).
16. C. E. Max, *Phys. Fluids* **19** (1), 74–77 (1976).
17. B. I. Cohen et al., *Phys. Fluids B* **3** (3), 766–775 (1991).
18. D. Bauer, P. Mulser, and W. H. Steeb, *Phys. Rev. Lett.* **75** (25), 4622–4625 (1996); G. Bonnaud, H. S. Brandi, C. Manus, G. Mainfray, et al., *Phys. Plasmas* **1** (4), 968–989 (1994); G. Sun et al., *Phys. Fluids* **30** (2), 526–532 (1987).
19. R. L. Berger et al., *Phys. Fluids B* **3** (1), 3–12 (1991).
20. B. I. Cohen et al., "Resonantly Excited Nonlinear Ion Waves," submitted to *Phys. Plasmas* (1996).